Physics of Plasmas

# Angular streaking of betatron X-rays in a transverse density gradient laser-wakefield accelerator

Cite as: Phys. Plasmas **25**, 113105 (2018); https://doi.org/10.1063/1.5054807
Submitted: 03 September 2018 . Accepted: 26 October 2018 . Published Online: 09 November 2018

Y. Ma, D. Seipt, S. J. D. Dann, M. J. V. Streeter, C. A. J. Palmer, L. Willingale, and A. G. R. Thomas

# Angular streaking of betatron X-rays in a transverse density gradient laser-wakefield accelerator

Y. Ma,[1,2,3,a)] D. Seipt,[1,2,3] S. J. D. Dann,[1,2] M. J. V. Streeter,[1,2] C. A. J. Palmer,[1,2] L. Willingale,[1,2,3] and A. G. R. Thomas[1,2,3]
[1]*Physics Department, Lancaster University, Bailrigg, Lancaster LA1 4YB, United Kingdom*
[2]*The Cockcroft Institute, Keckwick Lane, Daresbury WA4 4AD, United Kingdom*
[3]*Center for Ultrafast Optical Science, University of Michigan, Ann Arbor, Michigan 48109, USA*

(Received 3 September 2018; accepted 26 October 2018; published online 9 November 2018)

In a plasma with a transverse density gradient, laser wavefront tilt develops gradually due to phase velocity differences in different plasma densities. The wavefront tilt leads to a parabolic trajectory of the plasma wakefield and hence the accelerated electron beam, which leads to an angular streaking of the emitted betatron radiation. In this way, the temporal evolution of the betatron X-ray spectra will be converted into angular "streak," i.e., having a critical energy-angle correlation. An analytical model for the curved trajectory of a laser pulse in a transverse density gradient is presented. This gives the deflection angle of the electron beam and the betatron X-rays as a function of the plasma and laser parameters, and it was verified by particle-in-cell simulations. This angular streaking could be used as a single-shot diagnostic technique to reveal the temporal evolution of betatron X-ray spectra and hence the electron acceleration itself. *Published by AIP Publishing*. https://doi.org/10.1063/1.5054807

## I. INTRODUCTION

In laser-wakefield acceleration (LWFA),[1] electrons are trapped and accelerated in the plasma wake driven by the ponderomotive force of the laser pulse. During the acceleration, electrons perform transverse oscillations, termed betatron oscillations, due to the inherent transverse focusing force of the plasma wakefield, and produce synchrotron-like radiation, which is often referred to as "betatron" X-ray radiation.[2–4]

The plasma density distribution affects the evolution of the drive laser pulse[5] and hence the evolution of the wakefield and the behavior of the trapped electron bunch.[6] For example, a radial density gradient in a capillary has been used to overcome diffraction and guide the laser over a longer acceleration length[7] and to realize a plasma undulator when the laser pulse was injected off-axis.[8,9] A longitudinal density gradient has been used to realize density transition injection with a density down-ramp,[10–13] to compress the energy spread of the electron beam,[14] to tune the electron energy,[15] and to produce atto-second electron bunches with a density up-ramp.[16] The tilted density ramp[17] and transverse density gradient[18] have been used to enhance the betatron oscillation amplitude of the electron beam and hence the betatron X-rays. A combined density down-ramp and up-ramp was even used to realize rephasing to further increase the energy gain.[19] In these examples, the electron beam quality and dynamic behavior could be modulated and determined by the plasma density distribution.

The characteristics of the betatron X-rays are determined entirely by the characteristics of the electron beam and the Liénard-Wiechert potentials[20] in the classical field limit. From the Liénard-Wiechert potentials, the instantaneous radiation spectrum of the betatron oscillations can be derived. In the highly nonlinear "bubble" regime[21,22] of LWFA, the radiation spectrum is similar to that of the "wiggler" regime of synchrotron radiation with a characteristic parameter $K \gg 1$. Here, $K = \gamma\omega_\beta r_\beta/c$ describes the strength of the betatron oscillation of an electron with energy of $\gamma m_e c^2$ and the oscillation amplitude of $r_\beta$, $\omega_\beta = \omega_p/\sqrt{2\gamma}$ is the betatron oscillation frequency with a plasma frequency of $\omega_p = \sqrt{n_p e^2/\epsilon_0 m_e}$ at the plasma density $n_p$. The critical photon energy of the synchrotron-like spectrum[4] is $\hbar\omega_c = \frac{3}{2}\hbar\omega_\beta K\gamma^2$. The divergence angles of the betatron X-rays in the oscillation plane and the plane perpendicular to it are $\theta_\parallel = K/\gamma$ and $\theta_\perp = 1/\gamma$, respectively.[4] The average number of photons is given by $N_{\text{photon}} \simeq 0.033 N_e N_\beta K$, where $N_e$ is the number of electrons and $N_\beta$ is the number of periods of betatron oscillation. These properties make betatron X-rays a promising diagnostic of the acceleration dynamics. Betatron X-rays have previously been used to diagnose electron beam characteristics such as deducing the electron beam diameter,[23] transverse beam emittance,[24–26] and general LWFA dynamics.[27–30]

Here, we propose a method to measure the temporal evolution of betatron X-ray spectra in a single shot via spatial streaking. The streaking of the betatron X-rays is a result of the curved electron beam trajectory due to the laser wavefront tilt. The laser wavefront tilt is caused by the transverse laser phase velocity difference present when a laser propagates in a plasma with a transverse density gradient. Due to the strong dependence between X-rays and electron parameters, the streaked betatron X-rays could be a promising tool to reveal the evolution of electron beam.

Electrons in the plasma wakefield will gain energy in the acceleration phase and lose energy in the deceleration phase, and therefore, the characteristics of the betatron

a)Electronic mail: yongm@umich.edu

X-rays will also vary as the electron energy varies. However, almost all of the betatron X-ray spectra measured in experiments were simply the integration of the emission during the whole acceleration process,[30–34] even for those experiments with length-adjustable targets.[35,36] The critical photon energies were obtained by fitting the experimental results to the photon energy spectrum, either $dI/d\omega \simeq \omega/\omega_c \int_{\omega/\omega_c}^{\infty} K_{5/3}(\xi)d\xi$ for all photons or $d^2I/d\omega d\Omega|_{\theta=0} \simeq (\omega/\omega_c)^2 K_{2/3}^2(\omega/\omega_c)$ for on-axis photons, where $K_{5/3}$ and $K_{2/3}$ are the modified Bessel functions of the second kind. These operations are only valid for an electron beam without acceleration. With the consideration of electron acceleration, in principle, the instantaneous photon spectrum could be obtained by gradually changing the acceleration length $L_n$. The signal produced between the time interval $t_{n-1}$ to $t_n$ is given by the difference between the total signals at $L_{n-1}$ from that of $L_n$. However, this method can only be done by the combination of multiple shots and requires high shot-to-shot stability, which is still a challenge for LWFA. Therefore, to the best of our knowledge, no experimental effort has been made to resolve the temporal evolution of the betatron X-ray spectra.

Note that laser wavefront tilt has been deliberately induced[32,37,38] to control the betatron oscillation. However, in these works, the plasma density was homogeneous and the average deviation angle of the laser pulse direction remained constant during the laser plasma interaction, and hence, betatron streaking was not achievable and not investigated.

## II. THEORETICAL MODELING OF THE STREAKING IN A TRANSVERSE DENSITY GRADIENT

The laser pulse will be launched into a plasma region which has a density gradient $n_p(y)$ perpendicular to the initial laser propagation direction. The transverse density gradient causes a transverse phase velocity gradient, $v_{pL} = c/\sqrt{1 - n_p(y)/n_{cr}}$, for the drive laser pulse which eventually causes a laser wavefront tilt. The wavefront tilt will steer the drive laser pulse towards lower density regions, gradually changing its direction, see for instance Fig. 1(a).

The wakefield produced by the laser pulse follows a curved path, as does the electron bunch being accelerated in the wakefield. This is a correlation between time and the angle of the electrons' momentum vector. Since the X-rays are emitted within a small cone around the electron propagation direction, there is also a correlation between the angle of X-ray emission and the time of emission, leading to a streaked signal. As the electrons are accelerated, the X-ray critical energy changes. By measuring the critical energy along the streaked signal, the time-varying electron energy can be inferred.

To understand the angle-time correlation, we need to know how the laser pulse evolves as it propagates through the plasma. Since the wavefront tilt being caused by the transverse density gradient is an example of refraction, we may use Snell's law, $\mathrm{d}(\nu \cos\alpha)/\mathrm{d}x = 0$ by assuming that the gradient is formed by plasma slabs of constant density, with the grazing angle $\alpha$, $\tan\alpha = \mathrm{d}y/\mathrm{d}x$, and $\nu = c/v_{pL}$ is the refractive index of the plasma. Solving these equations for a linear transverse density gradient $n_p(y) = n\left(1 + \frac{y}{L}\right)$ yields a parabolic trajectory

$$y(x) = -\Phi(x^2 - 2xx_s), \tag{1}$$

where $\Phi = n/(4Ln_{\mathrm{cr}}\cos^2\alpha_0)$ and $x_s = \tan\alpha_0/2\Phi$. Here, $n$ refers to the plasma density at the point where the laser is injected into the plasma at $x = y = 0$, and $\alpha_0$ is the injection angle of the laser pulse with regard to the x axis. This is sufficient to describe the laser propagation in the plasma ramp in the quasi-linear regime $a_0 \lesssim 1$. In the bubble regime $a_0 > 1$, however, the laser pulse rapidly evolves as it propagates through the plasma.[5] In order to model the curved trajectory of the laser pulse we need to include the red-shift of laser wavelength ("photon deceleration") because the laser ponderomotive potential inflicts a longitudinal refractive index gradient at the position of the laser pulse. The red-shift causes the (effective) critical density to decrease as the laser propagates through the plasma causing a stronger refractive index gradient and, hence, a stronger bend of the laser trajectory. The red-shift rate can be modeled as[39] $\mathrm{d}\lambda/\mathrm{d}x = \sigma a_0 (n_p/n_{\mathrm{cr}})^{3/2}$, where the scaling can be derived from the non-linear 1D wave theory.[6,40] The scale factor $\sigma$ appears because the strength of the longitudinal gradient depends on the distance from the rising edge of the laser pulse, evoking a variable red-shift for different parts of the laser pulse. We refrain from a detailed description of these effects (e.g., by studying the evolution of the Wigner function of the laser pulse[5,22]) and instead condense the relevant physics to a single position dependent parameter. By solving the differential equations numerically, we determine the laser pulse trajectory $y(x)$, the deflection angle $\theta(x)$ and the red-shifted laser wavelength $\lambda(x)$ simultaneously and self-consistently. Choosing the constant as $\sigma = 0.17$ we find excellent agreement between the model and 2D Particle-in-Cell (PIC) simulations for both the laser trajectory and the red-shift in the leading part of the pulse. This strongly indicates that just the leading part of the pulse determines the curvature of the laser trajectory in the transverse plasma gradient with the rest of the laser pulse and the wakefield following behind.

To model the electron energy gain we assume a quasi-1D motion ($\theta \ll 1$) and solve the Lorentz force equation for the electrons

$$\frac{dx}{dt} = \beta_x c\,, \quad \frac{d\gamma}{dt} = -\beta_x \frac{\hat{e}_x}{R}(x - \beta_\phi ct), \tag{2}$$

in a static spherical ion cavity of radius $R = 2\sqrt{a_0}/k_p$ moving with velocity $\beta_\phi = 1 - 3\omega_p^2/2\omega_L^2$ and with normalized accelerating field[22] $\hat{e}_x = \omega_p\sqrt{a_0}$.

By injecting the electrons with initial energy $\gamma_0 = 1/\sqrt{1 - \beta_\phi^2}$ near the rear of the bubble $x - \beta_\phi ct = 0.95R$, at the end of the injection stage (see below), we find good agreement with 2D PIC simulations before dephasing. However, the above model fails for later stages when the wakefield bubble evolves rapidly causing dephasing much earlier than predicted by the static ion cavity model behind Eq. (2). A thorough description of the electron energy gain

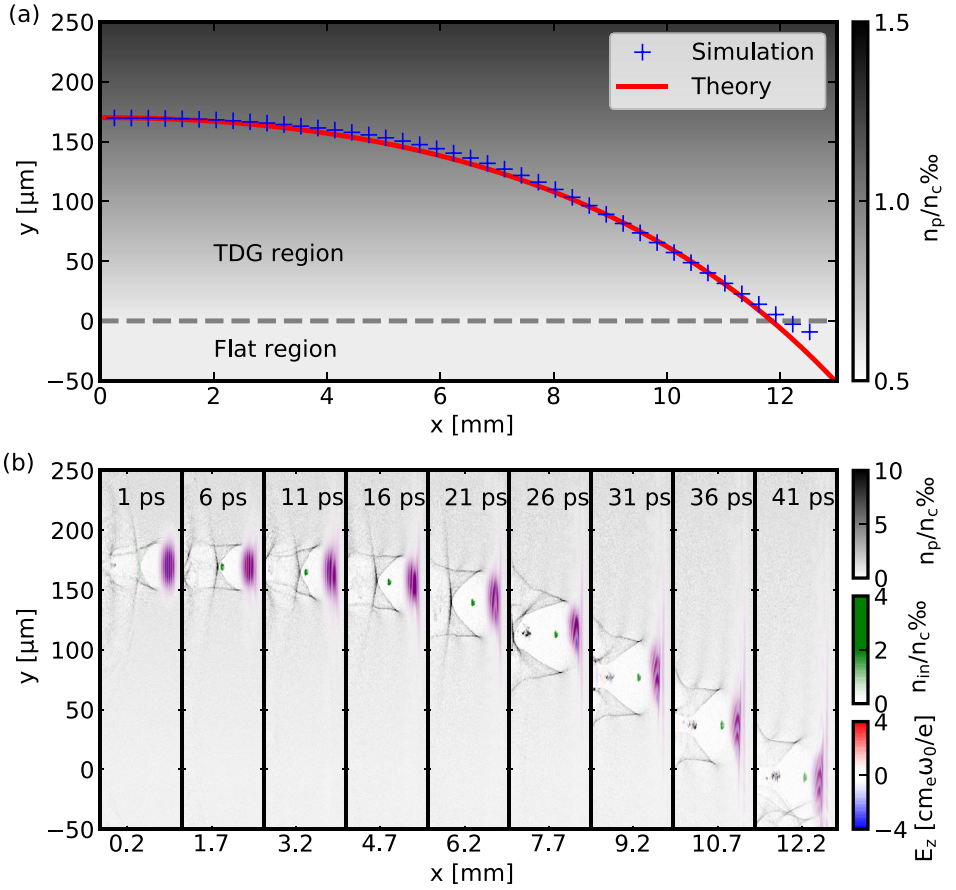


FIG. 1. (a) Plasma density distribution and the laser pulse trajectory predicted by the theoretical model (red line) and from the simulation (blue crosses). (b) Snapshots of the evolution of the laser pulse, the background plasma density, and the injected electron beams.

would require modeling of the laser pulse compression and other effects influencing the bubble expansion.

As mentioned above, the critical photon energy is a function of electron energy $\gamma$ and the plasma density $n_p$ as

$$\omega_c = \frac{3}{2}\omega_\beta K\gamma^2 = \frac{3}{4}\frac{e^2}{\epsilon_0 m_e c} r_\beta n_p \gamma^2 . \tag{3}$$

Therefore, with a known plasma density distribution, the betatron critical energy will be determined only by the electron energy while assuming the well-known scaling for the betatron amplitude[41] $r_\beta \sim (\gamma n_p)^{-1/4}$. Together with $\gamma(x)$ and $\theta(x)$ this uniquely determines the streaking trace $\omega_c(\theta)$. This works the other way around as well: For a given (or measured) streaking trace $\omega_c(\theta)$, together with $\theta(x)$, we can find $\gamma(x)$ and hence determine the dephasing point.

Using the analytic model above we can derive analytic scalings for the streaking speed—how much the electron energy or the betatron critical frequency change as the angle $\theta$ sweeps a certain value. This provides analytical scaling relations for how the laser pulse and plasma density gradient parameters affect the streaking.

By combining the equations for the electron energy gain and Snell's law we determine how much energy the electron gains per angular streak

$$\frac{\Delta\gamma}{\Delta\theta[\mathrm{mrad}]} \simeq 0.012\gamma_{p0}\frac{L}{\lambda_L}\sqrt{a_0} \approx 230, \tag{4}$$

where the last value refers to the parameters for which we performed PIC simulations (Sec. III A). For fast streaking this value should be as small as possible such that the angle changes a lot for a small change of $\gamma$. This can be realized, for instance, with a steeper density gradient, i.e., smaller values of $L$.

What is more relevant is the streaking speed for the critical betatron frequency: How much does the emission angle change for a variation in the critical frequency of the betatron spectrum

$$\frac{\Delta\theta[\mathrm{mrad}]}{\Delta\omega_c/\omega_c} = \frac{\frac{1000}{7\pi}\frac{\gamma}{\gamma_{p0}}\frac{\lambda_L}{L}\frac{1}{\sqrt{a_0}}}{1+\frac{3}{14\pi}(\gamma_{p0}\theta)\frac{\lambda_L}{L}\frac{\gamma}{\sqrt{a_0}}} \approx \frac{0.0025\gamma}{1+3.5\cdot 10^{-6}\gamma\theta[\mathrm{mrad}]}, \tag{5}$$

where the second line is again for the parameters considered in Sec. III A. Here, larger values mean better angular resolution of different frequencies. The streaking is relatively slow at the beginning of the acceleration when $\gamma \approx \gamma_{p0}$ and becomes faster in later stages when $\gamma \gg \gamma_{p0}$. Steeper gradients and smaller $a_0$ are beneficial, as well as small grazing angles.

## III. SIMULATION RESULTS

### A. Betatron streaking with parallel incidence

To verify the theoretical model, 2D PIC simulations were performed by using the EPOCH code[42] with the quantum electrodynamics (QED) module[43] to generate betatron

radiation directly without post-processing. The simulation box with the moving window is $300\,\mu\text{m} \times 100\,\mu\text{m}$ with $600 \times 2500$ cells in the $y$ and $x$ directions, where $y$ is the transverse direction and $x$ is the laser propagating direction, while the laser is polarized in the $z$ direction. The laser pulse shape is Gaussian in both transverse and longitudinal directions with a wavelength of $\lambda_L = 2\pi c/\omega_L = 800\,\text{nm}$, a full width at half maximum (FWHM) pulse duration of $\tau = 45$ fs, a $1/e^2$ spot size of $w_0 = 16.7\,\mu\text{m}$, and a peak amplitude of the normalized vector potential of $a_0 = 5.7$. To better control the electron injection, we employ an ionization injection scheme[44–51] with 1% partially ionized nitrogen $N^{5+}$ in a $500\,\mu\text{m}$ long injection stage added to the background electron plasma. This localization of the injection minimizes the energy spread of the accelerated electron beam. To avoid massive low-energy photons from low-energy background electrons, the QED module was modified to suppress photon emission from electrons with energy below a certain threshold, which is $\gamma = 200$ in the simulation here. Moreover, the QED module was only switched on for the ionized electrons. There are 5 macro-particles for each species per cell.

The transverse density distribution of the background plasma, as shown in Fig. 1(a), can be expressed as

$$n_p = \begin{cases} n_0\left(1 + \dfrac{y}{L}\right), & y > 0 \\ n_0, & y \leqslant 0, \end{cases} \tag{6}$$

where $n_0 = 1 \times 10^{18}\,\text{cm}^{-3}$, and $L = 200\,\mu\text{m}$ is the length over which the plasma density increases by $n_0$, i.e., the density gradient is $k = n_0/L = 5 \times 10^{15}\,\text{cm}^{-3}/\mu\text{m}$.

The general scenario of the simulation is illustrated in Fig. 1. Figure 1(a) gives the laser pulse trajectory predicted by the theory as well as that from the simulation. It is clear that the theoretically predicted trajectory fits very well with the simulation results which indicate that the betatron streaking can be well controlled. Figure 1(b) shows the snapshots of the distribution of the laser pulse and plasma density. As we can see that the deflection of the laser pulse is relatively slow, a 200-$\mu$m displacement over a 12-mm propagation distance. This preserves the stable acceleration and the injected electron beams remain transversely in the middle of the bubble. Thus collective high amplitude oscillation, often observed with transverse inhomogeneous plasma,[9,52] which changes the electron beam characteristics, was avoided.

As the laser pulse propagation angle changes at each time step, the corresponding pointing angle of the betatron X-rays changes accordingly, thus the temporal spectrum is dispersed into the streaked angular distribution. Since the electron energy evolves during the acceleration and deceleration, the corresponding critical photon energy as a function of the pointing angle should have the same trend. The streaked angular spectrum of betatron X-rays at the end of the simulation is shown in Fig. 2. The parabolic shape of the energy-angle correlation shows a clear trend of increase-then-decrease of the critical photon energy as the deflection angle increases. This indicates the acceleration-then-deceleration process of the electron beam. For a simple example, those photons with the maximum critical energy at the angle

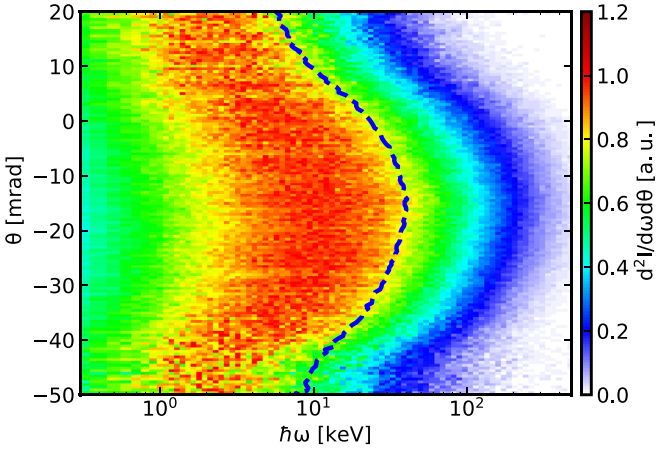


FIG. 2. Streaked angular spectrum at the end of the simulation. For each angle, the spectrum was normalized to its maximum. The blue dashed line represents the critical photon energy for each angle, fitted with the synchrotron spectrum.

$\theta_{\max} = -15$ mrad were emitted at this time when the electron beam reaches the dephasing point. By using the analytic model for the laser trajectory $\theta(x)$, we determine that the dephasing point is at $x = 7$ mm, or at $t = 23.3$ ps, which is consistent with the PIC simulation result shown in Fig. 4(b).

As mentioned above, almost all of the betatron X-ray spectra measured in experiments so far were simply time integrated, while the transverse density gradient scheme studied here allows the measurement of instantaneous emission from the electron beam at any time during the acceleration process. A typical instantaneous betatron X-ray spectrum (within a time step of 1 ps) was shown in Fig. 3(a).

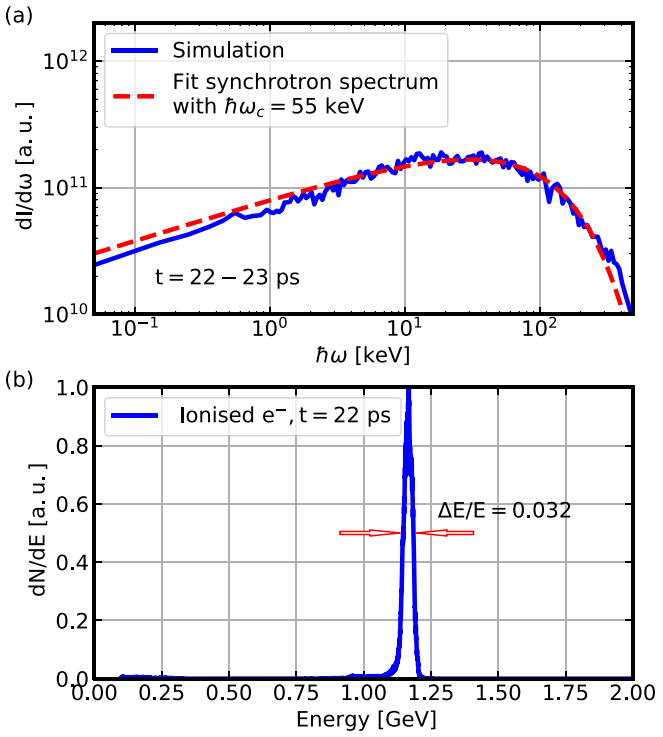


FIG. 3. Typical betatron radiation spectrum (a) and electron spectrum (b) at the dephasing point. The simulated betatron spectrum in (a) was fitted with the synchrotron spectrum $\omega/\omega_c \int_{\omega/\omega_c}^{\infty} K_{5/3}(\xi)d\xi$ (red curve) which gave a photon critical energy of $\omega_c = 55\,\text{keV}$.

As we can see, the spectrum from the simulation fits perfectly with the theoretical synchrotron spectrum. This is because the electron beam is mono-energetic, as shown in Fig. 3(b) which shows the electron spectrum at the dephasing point with a small energy spread of $\Delta E/E = 3.2\%$, and because, during a time-step of 1 ps, the energy changes of the electron beam are always less than 100 MeV, as shown in Fig. 4(a).

Figure 4(a) gives the evolution of electron peak energy $\gamma(t)$ from simulations and predicted by theory. As mentioned above, the theory failed to predict the energy gain near and beyond the dephasing point due to the rapid bubble evolution. Provided with $\gamma(t)$, the evolution of critical photon energy agrees with Eq. (3) [Fig. 4(b)] with a fitted $r_\beta(t) \sim (\gamma(t) n_p(t))^{-1/4}$ [inset of Fig. 4(b)]. The agreement between the simulation results (except for the last two time steps) and the theoretical prediction indicates that the transverse betatron oscillation amplitude is predictable, which can be used to estimate beam emittance together with the beam divergence angle in the direction perpendicular to the streaking direction. The deviation of the last two time steps is due to the fact that, at those time steps, the laser pulse has come out from the transverse density gradient region and the abrupt change of the plasma density induces high amplitude collective oscillations which increase the critical energy of photons.

The evolution of the angular distribution of photons emitted within each time step is shown in Fig. 4(c). As we can see, the mean deviated angle of the radiation is close to that predicted by the theory.

From Fig. 4(c), although the mean deviated angle of the betatron radiation at each time step can be well predicted, the instantaneous divergence angle of the betatron radiation is comparable to the deviated angle which lowers the spatial resolution and makes it challenging to resolve the temporal evolution in an experiment. Besides, with a continuously decreasing plasma density witnessed by the laser pulse, the plasma wavelength will increase continuously as $\lambda_p \propto 1/\sqrt{n_p}$ (see Fig. 5). The increase in the plasma wavelength causes fast dephasing, which lowers the maximum energy gain of the electron beam, as well as supporting continuous self-injection.[53–55] Self-injection should be avoided since it is not controllable and will increase the background noise of betatron X-rays.

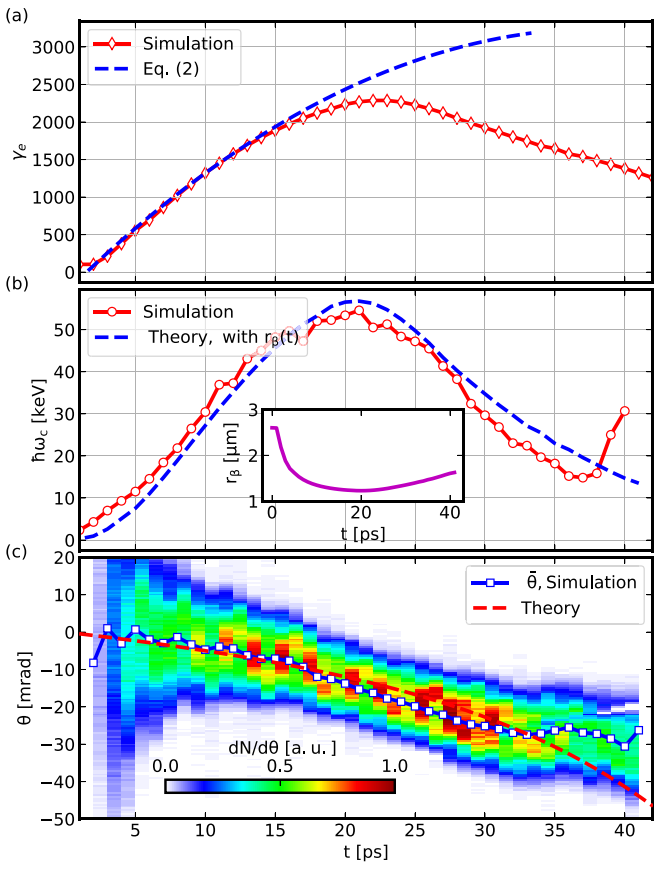


FIG. 4. (a) Evolution of the peak energy of the electron beam from the simulation (red diamonds) and theory (blue dash line). (b) Evolution of the critical energy of betatron X-rays from the simulation (red circles) and theory (blue dash line). The inset figure shows the theoretical evolution of betatron oscillation amplitudes based on the evolution of electron energy $\gamma_e(t)$ and plasma density $n_p(t)$ which gives the best fitting of critical energy. (c) Evolution of betatron X-ray angular distribution. The blue squares represent the mean deviated angle of the radiation and the red dash line represents the deviated angle of the laser pulse predicted by the theory.

## B. Betatron streaking with grazing incidence

A modified scheme with grazing incidence can be used to improve the performance of the betatron streaking, i.e., increasing the spatial resolution by lowering the divergence angle of the betatron radiation, and suppressing the self-injection and enlarging maximum energy gain of the electron beam (hence the betatron critical energy) via rephasing.

The basic idea of the modified scheme is to launch the laser pulse along the inverse trajectory in Fig. 1(a) from the low density region to the high density region with a small grazing angle $\alpha_0$ between the laser pulse and the direction perpendicular to the density gradient. The initial laser-target geometry is shown in Fig. 6(a) with a grazing incident angle $\alpha_0 = 25$ mrad. The density gradient is changed to $k = 1 \times 10^{16}\,\mathrm{cm}^{-3}/\mu\mathrm{m}$, while $n_0$ is the same with that in Fig. 1(a). The simulation box is enlarged to 750 $\mu$m in the $y$ direction. The laser intensity is lowered to $a_0 = 4$ as to match the lower initial plasma density. Before the laser pulse penetrate

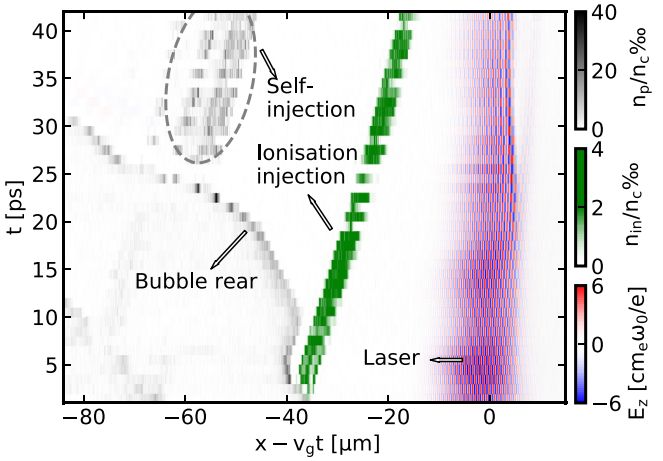


FIG. 5. Evolution of the laser pulse, plasma density distribution, and trapped electron beam. At each time step, these quantities were taken as a horizontal lineout at the centroid of the laser pulse.

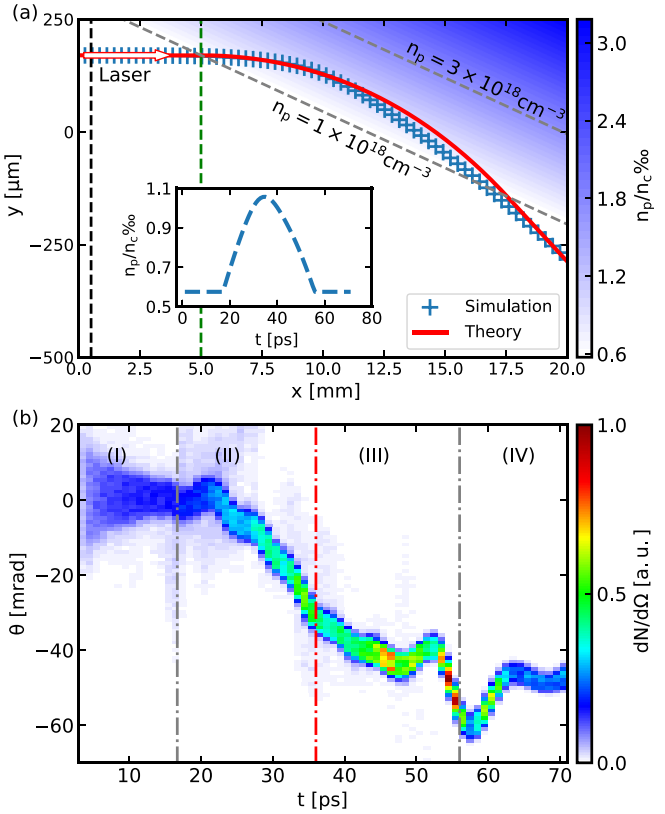


FIG. 6. (a) Plasma density distribution and the laser pulse trajectory. The balk and green dash lines characterise the length of the injection region and the pre-acceleration region, respectively. The gray dash line separates the homogeneous density region and the transverse density gradient region. The inset represents the local plasma density witnessed by the laser pulse. (b) Evolution of the instantaneous betatron radiation angular distribution. The four regions separated by the dash lines represent the four different interaction stages in which the plasma density distribution witnessed by the laser pulse is (I) homogeneous, (II) up-ramp, (III) down-ramp, and (IV) homogeneous, respectively.

into the density ramp region, a 5 mm long homogeneous plasma region was deliberately set to pre-accelerate the trapped electron beam. The reason for the pre-acceleration stage is that if the laser pulse was directly launched into a density up-ramp, the rapid increase in the plasma density will cause the rapid decrease in the plasma wavelength and the phase velocity of the wakefield which eventually enlarge the injection threshold and might lead to the failure of injection. We found that, for the laser-plasma parameters here, the optimal length of the pre-acceleration stage is 5 mm.

Figure 6(a) illustrates the laser pulse trajectory in the plasma gradient. One can clearly see that after it penetrated into the transverse density gradient region, the laser pulse was deflected by the plasma as was observed in Fig. 1(a) and left the transverse density gradient region eventually. The local plasma density witnessed by the laser pulse is shown in the inset figure of Fig. 6(a) which demonstrated the four-stage flat-upramp-downramp-flat density evolution. The betatron streaking was improved significantly with regard to the instantaneous divergence angle and maximum deviated angle, as shown in Fig. 6(b), compared with that in Fig. 4(c) with a monotonic decreasing plasma density. The changing of the outgoing direction of the betatron radiation is almost linear in the density up-ramp stage with a small instantaneous divergence angle with makes the scheme reliable in reality. The oscillation of the deviated angle at a later stage, especially when the laser pulse crossing the transition region between the transverse density gradient and homogeneous plasma is caused by the induced large amplitude collective oscillation as we mentioned above. To avoid this, one can simply terminate the interaction by reducing the plasma length. In comparison, the peak electron energy is slightly higher in the modified scheme even with a lower $a_0$, as we can see from Fig. 8(b). In fact, the electron peak energy, as well as the critical energy of photons, could be further increased with a different grazing angle $\alpha$ which will be illustrated below in Fig. 10.

The most important advantage of the modified scheme with a transverse density gradient is the realization of controlled rephasing.[19] In the density up-ramp region, the plasma wavelength decreases as the plasma density increases. As a result, the plasma bubble rear moves forward, reducing its distance to the trapped electron beam, as one can see from Fig. 7 (II). As we know, the longitudinal electrostatic field $E_x$ is almost linear inside the plasma bubble and the further from the bubble central, the higher the accelerating field strength. Therefore, the plasma density up-ramp will cause the enhancement of the accelerating field strength witnessed by the electron beam and hence enlarging the energy gain. The rephasing was confirmed by performing a benchmark run with a homogeneous plasma density while all the other laser and plasma parameters were kept the same. As shown in Fig. 8(a), during the whole density up-ramp stage, the accelerating field strength witnessed by the electron beam in the transverse density gradient case is much higher than that with homogeneous plasma. As a consequence, having entered the density up-ramp region, the electron peak energy in the transverse density gradient case becomes higher than that with a homogeneous plasma [Fig. 8(b)], which similarly impacts the critical energy of betatron photons [Fig. 8(c)]. Note that in Fig. 8(c), for both cases, the betatron critical energy evolution agrees with Eq. (3). Moreover, unlike what we observed in Figs. 1(b) and 5, the shrinking of the bubble in the density up-ramp region also

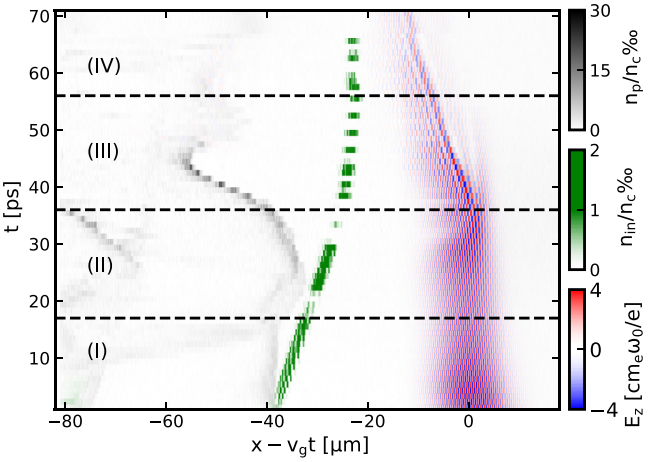


FIG. 7. Evolution of the laser pulse, plasma density distribution, and trapped electron beams.

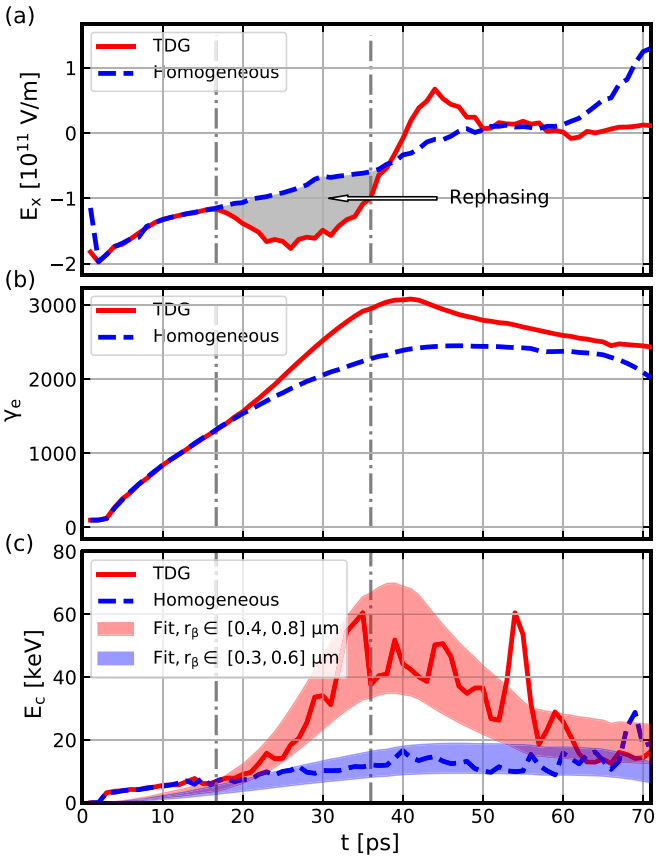


FIG. 8. (a) Comparison of the evolution of the instantaneous longitudinal electrostatic field witnessed by the trapped electron beam between the transverse density gradient and homogeneous plasma. The shadow represents the rephasing caused by the increasing plasma density. (b) Enhancement of electron peak energy due to rephasing. (c) Evolution of the critical energy of betatron radiation and its enhancement due to rephasing.

suppressed the self-injection as we observe no self-injection in Fig. 7.

The angular streaking of the betatron radiation could be used to determine the time evolution of the electron energy during the acceleration process. The retrieved electron energy as a function of propagation distance is shown in Fig. 9. For each angular lineout of the angularly resolved betatron spectrum, a critical frequency $\omega_c(\theta)$ was determined via the best fit to the synchrotron spectrum similar to Fig. 3(a). The curved laser pulse trajectory from the analytical model was used to relate each emission angle $\theta$ to a propagation distance. Note that in experiment, the curved laser pulse trajectory could be determined from optical probing. The unknown betatron oscillation amplitude could be determined from the betatron divergence angle[56,57] perpendicular to the density gradient which scales as $K/\gamma$. However, we do not have access to this from the 2D simulations. Here, therefore, we fix $r_\beta$ by fitting a model $\omega_c$ to the measured $\omega_c(\theta)$. From Fig. 9, one can see that the retrieved electron energy evolution is in reasonable agreement with the simulation results, which indicates the potential capability of the betatron streaking technique in diagnosing electron energy evolution.

The effect of varying grazing angle $\alpha_0$ on angular streaking was studied to optimize the characteristics of the electron beam and the betatron radiation. As we can see from Fig. 10,

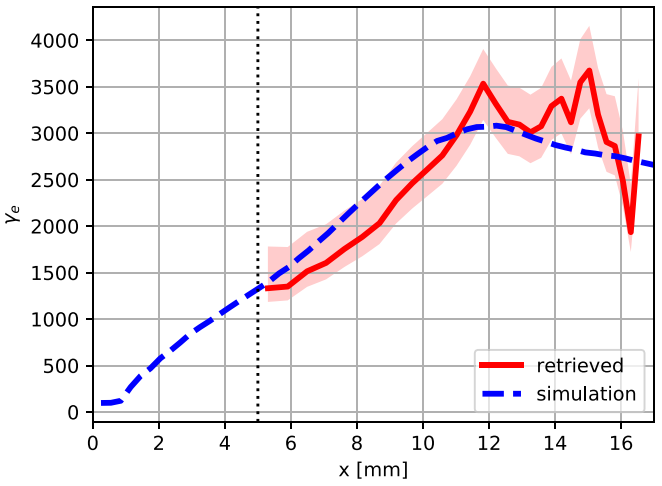


FIG. 9. Evolution of the electron energy as retrieved from the streaked betatron spectrum and compared to the PIC simulation results. Retrieval to the left of the dashed line is not possible since there is no betatron angular streaking due to the homogeneous plasma density before the laser pulse propagates into the transverse density gradient region at 5 mm [see Fig. 6(a)].

the evolution of the interaction can be well controlled with different grazing angles. In Fig. 10(b), the red shifting of the laser pulse develops faster with larger $\alpha_0$ which might be due to the much higher local plasma density witnessed by the

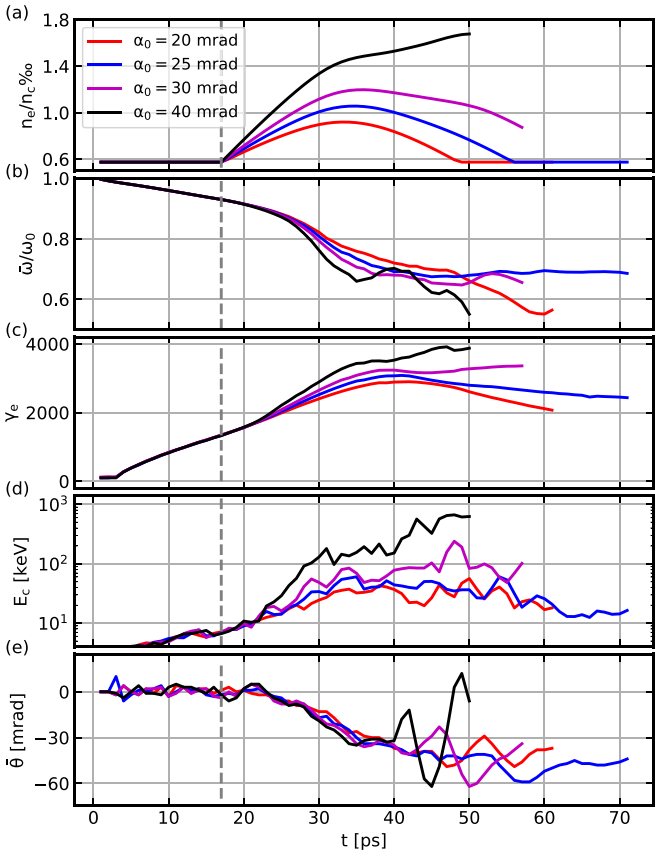


FIG. 10. Effects of the grazing angle $\alpha_0$ on the evolution of (a) local plasma density witnessed by the laser pulse, (b) laser pulse red-shifting where the average laser frequency was normalised to the laser frequency in vacuum $\omega_0$, (c) peak energy of the electron beam, (d) instantaneous critical energy of the betatron radiation, and (e) mean deviated angle of the betatron radiation. All the other laser and plasma parameters are the same for all the four runs and the same with that in Fig. 6(a).

laser pulse, as shown in Fig. 10(a). For higher $\alpha_0$, the local plasma density could increase continuously and the laser pulse cannot be deflected into the lower density region as the low $\alpha_0$ cases. As a consequence of enhanced rephasing with higher plasma density, the maximum energy gain increases reaching 2 GeV before the dephasing with $\alpha_0 = 40$ mrad in Fig. 10(c). The critical energy of the betatron radiation follows the same trend and could be close to 1 MeV with $\alpha_0 = 40$ mrad in Fig. 10(d). For larger $\alpha_0$, the mean deviated angle of betatron radiation is also slightly higher, as one can see from Fig. 10(e). Note that for a large $\alpha_0$, we observe large oscillations of the mean emission angle during the late stage. This could be avoided by terminating the interaction with shorter plasma length as mentioned above or by using a longitudinal density gradient.

## IV. CONCLUSION

In conclusion, a betatron streaking technique for LWFA has been proposed. With a transverse density gradient, the temporal evolution of the betatron X-ray spectrum can be retrieved from the angular streaking and the curved laser trajectory. A theoretical model was developed to predict the curved laser trajectory in a transverse density gradient and it was well verified by the PIC simulations. The betatron angular streaking has the potential to provide single shot diagnosis of the dynamic process of LWFA for which low shot-to-shot stability limits the usefulness of traditional multi-shot diagnostic techniques. It can also be used to isolate the X-rays from the electron beams without implementing any magnetic devices.

A qualitatively similar streaking of the emitted betatron X-rays is expected to occur for LWFA in a plasma channel when the beam is injected either off-axis or is not aligned properly. While the former case corresponds to the parallel incidence studied in Sec. III A, the latter corresponds to the grazing incidence discussed in Sec. III B. In this regard, the betatron streaking could be used as a diagnostic for alignment for instance in multi-stage LWFA schemes.[58]

In this paper, we discussed the principal physics of angular betatron streaking. We have shown that we can determine the longitudinal position of electron dephasing from the betatron spectrum. Retrieving more detailed information on the electron evolution requires—and is limited by—a precise theoretical modeling of the laser pulse trajectory propagating through the transverse gradient. However, experimentally the laser pulse and bubble trajectories could be imaged by Thomson scattering[59,60] and shadowgraphy.[61,62] Moreover, the accuracy of the electron energy evolution retrieval is rather sensitive to the energy spread of the electron beam due to the $\sim\gamma^{7/4}$ scaling of the critical photon energy to electron energy. Therefore, the retrieving technique would be more appealing for low energy spread electron beams.

The analytical scalings indicate a steeper plasma gradient means larger streaking speed, i.e., a better resolution of the different betatron frequencies. There are limitations to the gradients as well since for too steep gradients the assumptions of spherical ion cavities do not hold anymore. These limitations of the model should be addressed in a future work.

## ACKNOWLEDGMENTS

This work was supported by the STFC (No. ST/J002062/1) and Department of Energy Grant No. DE-SC0019186. The development of EPOCH was in part funded by the UK EPSRC Grant Nos. EP/G054950/1, EP/G056803/1, EP/G055165/1, and EP/M022463/1.

[1]T. Tajima and J. M. Dawson, "Laser electron accelerator," Phys. Rev. Lett. **43**, 267–270 (1979).
[2]E. Esarey, B. A. Shadwick, P. Catravas, and W. P. Leemans, "Synchrotron radiation from electron beams in plasma-focusing channels," Phys. Rev. E **65**, 056505 (2002).
[3]A. G. R. Thomas and K. Krushelnick, "Betatron x-ray generation from electrons accelerated in a plasma cavity in the presence of laser fields," Phys. Plasmas **16**, 103103 (2009).
[4]S. Corde, K. Ta Phuoc, G. Lambert, R. Fitour, V. Malka, A. Rousse, A. Beck, and E. Lefebvre, "Femtosecond x rays from laser-plasma accelerators," Rev. Mod. Phys. **85**, 1–48 (2013).
[5]M. J. V. Streeter, S. Kneip, M. S. Bloom, R. A. Bendoyro, O. Chekhlov, A. E. Dangor, A. Döpp, C. J. Hooker, J. Holloway, J. Jiang, N. C. Lopes, H. Nakamura, P. A. Norreys, C. A. J. Palmer, P. P. Rajeev, J. Schreiber, D. R. Symes, M. Wing, S. P. D. Mangles, and Z. Najmudin, "Observation of laser power amplification in a self-injecting laser wakefield accelerator," Phys. Rev. Lett. **120**, 254801 (2018).
[6]E. Esarey, C. B. Schroeder, and W. P. Leemans, "Physics of laser-driven plasma-based electron accelerators," Rev. Mod. Phys. **81**, 1229–1285 (2009).
[7]W. P. Leemans, B. Nagler, A. J. Gonsalves, C. Toth, K. Nakamura, C. G. R. Geddes, E. Esarey, C. B. Schroeder, and S. M. Hooker, "Gev electron beams from a centimetre-scale accelerator," Nat. Phys. **2**, 696–699 (2006).
[8]S. G. Rykovanov, C. B. Schroeder, E. Esarey, C. G. R. Geddes, and W. P. Leemans, "Plasma undulator based on laser excitation of wakefields in a plasma channel," Phys. Rev. Lett. **114**, 145003 (2015).
[9]M. Chen, J. Luo, F.-Y. Li, F. Liu, Z.-M. Sheng, and J. Zhang, "Tunable synchrotron-like radiation from centimeter scale plasma channels," Light Sci. Appl. **5**, e16015 (2016).
[10]S. Bulanov, N. Naumova, F. Pegoraro, and J. Sakai, "Particle injection into the wave acceleration phase due to nonlinear wake wave breaking," Phys. Rev. E **58**, R5257–R5260 (1998).
[11]H. Suk, N. Barov, J. B. Rosenzweig, and E. Esarey, "Plasma electron trapping and acceleration in a plasma wake field using a density transition," Phys. Rev. Lett. **86**, 1011–1014 (2001).
[12]K. Schmid, A. Buck, C. M. S. Sears, J. M. Mikhailova, R. Tautz, D. Herrmann, M. Geissler, F. Krausz, and L. Veisz, "Density-transition based electron injector for laser driven wakefield accelerators," Phys. Rev. ST Accel. Beams **13**, 091301 (2010).
[13]A. Buck, J. Wenz, J. Xu, K. Khrennikov, K. Schmid, M. Heigoldt, J. M. Mikhailova, M. Geissler, B. Shen, F. Krausz, S. Karsch, and L. Veisz, "Shock-front injector for high-quality laser-plasma acceleration," Phys. Rev. Lett. **110**, 185006 (2013).
[14]C. G. R. Geddes, K. Nakamura, G. R. Plateau, C. Toth, E. Cormier-Michel, E. Esarey, C. B. Schroeder, J. R. Cary, and W. P. Leemans, "Plasma-density-gradient injection of low absolute-momentum-spread electron bunches," Phys. Rev. Lett. **100**, 215004 (2008).
[15]A. J. Gonsalves, K. Nakamura, C. Lin, D. Panasenko, S. Shiraishi, T. Sokollik, C. Benedetti, C. B. Schroeder, C. G. R. Geddes, J. van Tilborg, J. Osterhoff, E. Esarey, C. Toth, and W. P. Leemans, "Tunable laser plasma accelerator based on longitudinal density tailoring," Nat. Phys. **7**, 862–866 (2011).
[16]F. Y. Li, Z. M. Sheng, Y. Liu, J. Meyer-ter Vehn, W. B. Mori, W. Lu, and J. Zhang, "Dense attosecond electron sheets from laser wakefields using an up-ramp density transition," Phys. Rev. Lett. **110**, 135002 (2013).
[17]C. Yu, J. Liu, W. Wang, W. Li, R. Qi, Z. Zhang, Z. Qin, J. Liu, M. Fang, K. Feng, Y. Wu, L. Ke, Y. Chen, C. Wang, Y. Xu, Y. Leng, C. Xia, R. Li, and Z. Xu, "Enhanced betatron radiation by steering a laser-driven plasma wakefield with a tilted shock front," Appl. Phys. Lett. **112**, 133503 (2018).

[18]J. Ferri and X. Davoine, "Enhancement of betatron X-rays through asymmetric laser wakefield generated in transverse density gradients," Phys. Rev. ST Accel. Beams **21**, 091302 (2018).
[19]E. Guillaume, A. Döpp, C. Thaury, K. Ta Phuoc, A. Lifschitz, G. Grittani, J.-P. Goddet, A. Tafzi, S. W. Chou, L. Veisz, and V. Malka, "Electron rephasing in a laser-wakefield accelerator," Phys. Rev. Lett. **115**, 155002 (2015).
[20]J. D. Jackson, *Classical Electrodynamics*, 3rd ed. (Willy, New York, 2001).
[21]A. Pukhov and J. Meyer-ter Vehn, "Laser wake field acceleration: The highly non-linear broken-wave regime," Appl. Phys. B **74**, 355–361 (2002).
[22]W. Lu, M. Tzoufras, C. Joshi, F. S. Tsung, W. B. Mori, J. Vieira, R. A. Fonseca, and L. O. Silva, "Generating multi-gev electron bunches using single stage laser wakefield acceleration in a 3d nonlinear regime," Phys. Rev. ST Accel. Beams **10**, 061301 (2007).
[23]M. Schnell, A. Sävert, B. Landgraf, M. Reuter, M. Nicolai, O. Jäckel, C. Peth, T. Thiele, O. Jansen, A. Pukhov, O. Willi, M. C. Kaluza, and C. Spielmann, "Deducing the electron-beam diameter in a laser-plasma accelerator using x-ray betatron radiation," Phys. Rev. Lett. **108**, 075001 (2012).
[24]S. Kneip, C. McGuffey, J. L. Martins, M. S. Bloom, V. Chvykov, F. Dollar, R. Fonseca, S. Jolly, G. Kalintchenko, K. Krushelnick, A. Maksimchuk, S. P. D. Mangles, Z. Najmudin, C. A. J. Palmer, K. T. Phuoc, W. Schumaker, L. O. Silva, J. Vieira, V. Yanovsky, and A. G. R. Thomas, "Characterization of transverse beam emittance of electrons from a laser-plasma wakefield accelerator in the bubble regime using betatron x-ray radiation," Phys. Rev. ST Accel. Beams **15**, 021302 (2012).
[25]G. R. Plateau, C. G. R. Geddes, D. B. Thorn, M. Chen, C. Benedetti, E. Esarey, A. J. Gonsalves, N. H. Matlis, K. Nakamura, C. B. Schroeder, S. Shiraishi, T. Sokollik, J. van Tilborg, C. Toth, S. Trotsenko, T. S. Kim, M. Battaglia, T. Stöhlker, and W. P. Leemans, "Low-emittance electron bunches from a laser-plasma accelerator measured using single-shot x-ray spectroscopy," Phys. Rev. Lett. **109**, 064802 (2012).
[26]G. Golovin, S. Banerjee, C. Liu, S. Chen, J. Zhang, B. Zhao, P. Zhang, M. Veale, M. Wilson, P. Seller, and D. Umstadter, "Intrinsic beam emittance of laser-accelerated electrons measured by x-ray spectroscopic imaging," Sci. Rep. **6**, 24622 (2016).
[27]S. Corde, C. Thaury, K. T. Phuoc, A. Lifschitz, G. Lambert, J. Faure, O. Lundh, E. Benveniste, A. Ben-Ismail, L. Arantchuk, A. Marciniak, A. Stordeur, P. Brijesh, A. Rousse, A. Specka, and V. Malka, "Mapping the x-ray emission region in a laser-plasma accelerator," Phys. Rev. Lett. **107**, 215004 (2011).
[28]G. Genoud, K. Cassou, F. Wojda, H. E. Ferrari, C. Kamperidis, M. Burza, A. Persson, J. Uhlig, S. Kneip, S. P. D. Mangles, A. Lifschitz, B. Cros, and C.-G. Wahlström, "Laser-plasma electron acceleration in dielectric capillary tubes," Appl. Phys. B **105**, 309 (2011).
[29]C. Thaury, E. Guillaume, S. Corde, R. Lehe, M. Le Bouteiller, K. Ta Phuoc, X. Davoine, J. M. Rax, A. Rousse, and V. Malka, "Angular-momentum evolution in laser-plasma accelerators," Phys. Rev. Lett. **111**, 135002 (2013).
[30]Y. Ma, L. M. Chen, N. A. M. Hafz, D. Z. Li, K. Huang, W. C. Yan, J. Dunn, Z. M. Sheng, and J. Zhang, "Diagnosis of bubble evolution in laser-wakefield acceleration via angular distributions of betatron x-rays," Appl. Phys. Lett. **105**, 161110 (2014).
[31]A. Rousse, K. T. Phuoc, R. Shah, A. Pukhov, E. Lefebvre, V. Malka, S. Kiselev, F. Burgy, J.-P. Rousseau, D. Umstadter, and D. Hulin, "Production of a kev x-ray beam from synchrotron radiation in relativistic laser-plasma interaction," Phys. Rev. Lett. **93**, 135005 (2004).
[32]S. P. D. Mangles, G. Genoud, S. Kneip, M. Burza, K. Cassou, B. Cros, N. P. Dover, C. Kamperidis, Z. Najmudin, A. Persson, J. Schreiber, F. Wojda, and C.-G. Wahlström, "Controlling the spectrum of x-rays generated in a laser-plasma accelerator by tailoring the laser wavefront," Appl. Phys. Lett. **95**, 181106 (2009).
[33]F. Albert, B. B. Pollock, J. L. Shaw, K. A. Marsh, J. E. Ralph, Y.-H. Chen, D. Alessi, A. Pak, C. E. Clayton, S. H. Glenzer, and C. Joshi, "Angular dependence of betatron x-ray spectra from a laser-wakefield accelerator," Phys. Rev. Lett. **111**, 235004 (2013).
[34]L. M. Chen, W. C. Yan, D. Z. Li, Z. D. Hu, L. Zhang, W. M. Wang, N. Hafz, J. Y. Mao, K. Huang, Y. Ma, J. R. Zhao, J. L. Ma, Y. T. Li, X. Lu, Z. M. Sheng, Z. Y. Wei, J. Gao, and J. Zhang, "Bright betatron x-ray radiation from a laser-driven-clustering gas target," Sci. Rep. **3**, 1912 (2013).
[35]S. Corde, C. Thaury, A. Lifschitz, G. Lambert, K. Ta Phuoc, X. Davoine, R. Lehe, D. Douillet, A. Rousse, and V. Malka, "Observation of longitudinal and transverse self-injections in laser-plasma accelerators," Nat. Commun. **4**, 1501 (2013).
[36]W. Yan, L. Chen, D. Li, L. Zhang, N. A. M. Hafz, J. Dunn, Y. Ma, K. Huang, L. Su, M. Chen, Z. Sheng, and J. Zhang, "Concurrence of monoenergetic electron beams and bright x-rays from an evolving laser-plasma bubble," Proc. Natl. Acad. Sci. U. S. A. **111**, 5825–5830 (2014).
[37]A. Popp, J. Vieira, J. Osterhoff, Z. Major, R. Hörlein, M. Fuchs, R. Weingartner, T. P. Rowlands-Rees, M. Marti, R. A. Fonseca, S. F. Martins, L. O. Silva, S. M. Hooker, F. Krausz, F. Grüner, and S. Karsch, "All-optical steering of laser-wakefield-accelerated electron beams," Phys. Rev. Lett. **105**, 215001 (2010).
[38]M. Schnell, A. Sävert, I. Uschmann, M. Reuter, M. Nicolai, T. Kämpfer, B. Landgraf, O. Jäckel, O. Jansen, A. Pukhov, M. C. Kaluza, and C. Spielmann, "Optical control of hard x-ray polarization by electron injection in a laser wakefield accelerator," Nat. Commun. **4**, 2421 (2013).
[39]Z. Nie, C.-H. Pai, J. Hua, C. Zhang, Y. Wu, Y. Wan, F. Li, J. Zhang, Z. Cheng, Q. Su, S. Liu, Y. Ma, X. Ning, Y. He, W. Lu, H.-H. Chu, J. Wang, W. B. Mori, and C. Joshi, "Relativistic single-cycle tunable infrared pulses generated from a tailored plasma density structure," Nat. Photonics **12**, 489–494 (2018).
[40]P. Sprangle, E. Esarey, and A. Ting, "Nonlinear theory of intense laser-plasma interactions," Phys. Rev. Lett. **64**, 2011–2014 (1990).
[41]A. G. R. Thomas, "Scalings for radiation from plasma bubbles," Phys. Plasmas **17**, 056708 (2010).
[42]T. D. Arber, K. Bennett, C. S. Brady, A. Lawrence-Douglas, M. G. Ramsay, N. J. Sircombe, P. Gillies, R. G. Evans, H. Schmitz, A. R. Bell, and C. P. Ridgers, "Contemporary particle-in-cell approach to laser-plasma modelling," Plasma Phys. Controlled Fusion **57**, 113001 (2015).
[43]C. Ridgers, J. Kirk, R. Duclous, T. Blackburn, C. Brady, K. Bennett, T. Arber, and A. Bell, "Modelling gamma-ray photon emission and pair production in high-intensity laser-matter interactions," J. Comput. Phys. **260**, 273–285 (2014).
[44]D. Umstadter, J. K. Kim, and E. Dodd, "Laser injection of ultrashort electron pulses into wakefield plasma waves," Phys. Rev. Lett. **76**, 2073–2076 (1996).
[45]M. Chen, Z.-M. Sheng, Y.-Y. Ma, and J. Zhang, "Electron injection and trapping in a laser wakefield by field ionization to high-charge states of gases," J. Appl. Phys. **99**, 056109 (2006).
[46]A. Pak, K. A. Marsh, S. F. Martins, W. Lu, W. B. Mori, and C. Joshi, "Injection and trapping of tunnel-ionized electrons into laser-produced wakes," Phys. Rev. Lett. **104**, 025003 (2010).
[47]C. McGuffey, A. G. R. Thomas, W. Schumaker, T. Matsuoka, V. Chvykov, F. J. Dollar, G. Kalintchenko, V. Yanovsky, A. Maksimchuk, K. Krushelnick, V. Y. Bychenkov, I. V. Glazyrin, and A. V. Karpeev, "Ionization induced trapping in a laser wakefield accelerator," Phys. Rev. Lett. **104**, 025004 (2010).
[48]J. S. Liu, C. Q. Xia, W. T. Wang, H. Y. Lu, C. Wang, A. H. Deng, W. T. Li, H. Zhang, X. Y. Liang, Y. X. Leng, X. M. Lu, C. Wang, J. Z. Wang, K. Nakajima, R. X. Li, and Z. Z. Xu, "All-optical cascaded laser wakefield accelerator using ionization-induced injection," Phys. Rev. Lett. **107**, 035001 (2011).
[49]B. B. Pollock, C. E. Clayton, J. E. Ralph, F. Albert, A. Davidson, L. Divol, C. Filip, S. H. Glenzer, K. Herpoldt, W. Lu, K. A. Marsh, J. Meinecke, W. B. Mori, A. Pak, T. C. Rensink, J. S. Ross, J. Shaw, G. R. Tynan, C. Joshi, and D. H. Froula, "Demonstration of a narrow energy spread, ~0.5 GeV electron beam from a two-stage laser wakefield accelerator," Phys. Rev. Lett. **107**, 045001 (2011).
[50]M. Mirzaie, S. Li, M. Zeng, N. A. M. Hafz, M. Chen, G. Y. Li, Q. J. Zhu, H. Liao, T. Sokollik, F. Liu, Y. Y. Ma, L. Chen, Z. M. Sheng, and J. Zhang, "Demonstration of self-truncated ionization injection for GeV electron beams," Sci. Rep. **5**, 14659 (2015).
[51]K. Huang, Y. F. Li, D. Z. Li, L. M. Chen, M. Z. Tao, Y. Ma, J. R. Zhao, M. H. Li, M. Chen, M. Mirzaie, N. Hafz, T. Sokollik, Z. M. Sheng, and J. Zhang, "Resonantly enhanced betatron hard x-rays from ionization injected electrons in a laser plasma accelerator," Sci. Rep. **6**, 27633 (2016).
[52]V. B. Pathak, J. L. Martins, J. Vieira, R. A. Fonseca, and L. O. Silva, "Laser wakefield acceleration in corrugated plasma channel," in *Proceedings of the 41st EPS Conference on Plasma Physics* (2014), Vol. 38F, p. P2.110.
[53]S. Y. Kalmykov, S. A. Yi, V. Khudik, and G. Shvets, "Electron self-injection and trapping into an evolving plasma bubble," Phys. Rev. Lett. **103**, 135004 (2009).

[54]S. Y. Kalmykov, A. Beck, S. A. Yi, V. N. Khudik, M. C. Downer, E. Lefebvre, B. A. Shadwick, and D. P. Umstadter, "Electron self-injection into an evolving plasma bubble: Quasi-monoenergetic laser-plasma acceleration in the blowout regime," Phys. Plasmas **18**, 056704 (2011).
[55]Y. Ma, L. Chen, D. Li, W. Yan, K. Huang, M. Chen, Z. Sheng, K. Nakajima, T. Tajima, and J. Zhang, "Generation of femtosecond $\gamma$-ray bursts stimulated by laser-driven hosing evolution," Sci. Rep. **6**, 30491 (2016).
[56]I. Kostyukov, S. Kiselev, and A. Pukhov, "X-ray generation in an ion channel," Phys. Plasmas **10**, 4818–4828 (2003).
[57]J. H. Jeon, K. Nakajima, H. T. Kim, Y. J. Rhee, V. B. Pathak, M. H. Cho, J. H. Shin, B. J. Yoo, S. H. Jo, K. W. Shin, C. Hojbota, L. J. Bae, J. Jung, M. S. Cho, J. H. Sung, S. K. Lee, B. I. Cho, I. W. Choi, and C. H. Nam, "Measurement of angularly dependent spectra of betatron gamma-rays from a laser plasma accelerator with quadrant-sectored range filters," Phys. Plasmas **23**, 073105 (2016).
[58]J. Luo, M. Chen, W. Y. Wu, S. M. Weng, Z. M. Sheng, C. B. Schroeder, D. A. Jaroszynski, E. Esarey, W. P. Leemans, W. B. Mori, and J. Zhang, "Multistage coupling of laser-wakefield accelerators with curved plasma channels," Phys. Rev. Lett. **120**, 154801 (2018).
[59]Y. Ma, L. M. Chen, M. H. Li, Y. F. Li, J. G. Wang, M. Z. Tao, Y. J. Han, J. R. Zhao, K. Huang, W. C. Yan, D. Z. Li, Z. Y. Chen, J. L. Ma, Y. T. Li, Z. M. Sheng, and J. Zhang, "Multiple quasi-monoenergetic electron beams from laser-wakefield acceleration with spatially structured laser pulse," Phys. Plasmas **22**, 083102 (2015).
[60]M. Mirzaie, N. A. M. Hafz, S. Li, F. Liu, F. He, Y. Cheng, and J. Zhang, "Enhanced electron yield from laser-driven wakefield acceleration in high-z gas jets," Rev. Sci. Instrum. **86**, 103502 (2015).
[61]A. Sävert, S. P. D. Mangles, M. Schnell, E. Siminos, J. M. Cole, M. Leier, M. Reuter, M. B. Schwab, M. Möller, K. Poder, O. Jäckel, G. G. Paulus, C. Spielmann, S. Skupin, Z. Najmudin, and M. C. Kaluza, "Direct observation of the injection dynamics of a laser wakefield accelerator using few-femtosecond shadowgraphy," Phys. Rev. Lett. **115**, 055002 (2015).
[62]S. Kuschel, M. B. Schwab, M. Yeung, D. Hollatz, A. Seidel, W. Ziegler, A. Sävert, M. C. Kaluza, and M. Zepf, "Controlling the self-injection threshold in laser wakefield accelerators," Phys. Rev. Lett. **121**, 154801 (2018).